On the relation between ionospheric winter anomalies and solar wind

Gian-Carlo Rumi
Via Cavour 17, Lecco, Italy

Abstract
There are two different winter anomalies. A small one that appears in connection with ionization at relatively low latitudes in the bottom of the *D*-region of the ionosphere. There, the electron densities in the winter happen to be less than should be expected. On the other hand, the classic winter anomaly is present when in the winter the upper *D*-region, again at relatively low latitudes, has more ionization than should be expected. Both these effects are due to the slant compression of the geomagnetic field produced by the solar wind in the winter season (which is, of course, the summer season when reference is made to events in the other hemisphere). It is shown that the small winter anomaly is a consequence of a hemispheric imbalance in the flux of galactic cosmic rays determined by the obliquely distorted geomagnetic field. It is shown that the standard winter anomaly can be ascribed to the influx of a super solar wind, which penetrates into the Earth's polar atmosphere down to *E*-region heights and, duly concentrated through a funneling action at the winter pole of the distorted geomagnetic field, slows down the winter polar vortex. An equatorward motion of the polar air with its content of nitric oxide brings about the excess of ionization in the upper *D*-region at lower latitudes. The experimentally observed rhythmic recurrence of the upper winter anomaly is correlated to a possible rhythmic recurrence of the super solar wind. The actual detection of the upper winter anomaly could yield some information on the velocity of the basic solar wind. A by-product of the present analysis, the determination of Γ, the coefficient of collisional detachment of the electrons from the O_2^- ions, is presented in the Appendix.

Key words *ionospheric winter anomalies – solar wind*

1. Introduction

There are two winter anomalies, a minor one relative to the bottom of the *D*-region of the ionosphere and a major one relative to the upper part of that region. How do they arise? Do the winter anomalies depend on the tilt of the Earth's polar axis over the ecliptic as the winter itself does?

In order to clarify the issue, a recollection of the characteristics and properties of the winter anomalies is here outlined. For the minor anomaly it is enough to say that at times the electron density in the lower part of the *D*-region at relatively low latitudes in the winter is less than should be expected. For the major and better known anomaly it should be said that the phenomenon consists in a significant enhancement of the electron density at altitudes between 80 and 90 km. It becomes manifest through an enhancement of the radio wave absorption. It appears to be confined to geomagnetic latitudes – northern and southern – between, say, 40° and 50°. It is a diurnal event and proper to the winter season, in the northern and in the southern hemisphere respectively. It is present even when

Mailing address: Dr. Gian-Carlo Rumi, Via Cavour 17, 23900 Lecco, Italy.

geomagnetic disturbances are absent. It is vaguely related to a warming of the stratosphere. Enhancements up to 5 times the normal value of the radio wave absorption have been observed. Winter anomaly is anticorrelated over large longitudinal differences.

The minor anomaly does not have much history. The major anomaly has been observed and studied for more than 60 years.

This phenomenon was first observed by Appleton (1937). Since then, many papers on this subject have appeared in the scientific literature. All of them explain the observed enhancement of the radio wave absorption as due to an increase of the electron density in the *D*-region of the ionosphere. But there is a distinct discrepancy about the origin of this phenomenon. Many authors suggest that a redistribution and transportation of particles by aeronomic or meteorological effects are to be seen as the cause of this anomaly. Some of these authors indicate a warming of the atmosphere, others the activity of planetary waves, still others the presence of wind currents, or a contribution of them as the triggering event of this phenomenon.

A different group of theories suggests that the classic winter anomaly is produced by the precipitation of energetic electrons. A complete list of references on this anomaly, updated to the year 1980 can be found in a paper by Sato (1980). The special issue of the *Journal of Atmospheric and Terrestrial Physics* of October/November 1979 deserves special consideration among the papers listed by Sato. It gives the findings of the experimentation carried out during the Western European Winter Anomaly Campaign 1975/1976. It offers the most complete and coherent set of data of this complex phenomenon. Hence, it was chosen to supply an experimental support to the deductions of the present paper, regarding the small and classic winter anomaly. Of the two subclasses of the classic winter anomaly (Garcia *et al.*, 1987), namely the «smooth» one (slight absorption enhancement) and the «sporadic» one (large absorption enhancement), only the second one will be studied here.

Of course, the research on the classic anomaly effects has been active even after 1980. Among the papers published since then and offering not only some insights into our phenomenon, but also some possibilities of confrontation with our findings, three of them were selected for ensuing comments: a first one that presents a scale analysis of the *D*-region winter anomaly, elaborated by the same group who operated during the above quoted Winter Anomaly Campaign (Offermann *et al.*, 1982); a second one that explains how the transport of Nitric Oxide in the *D*-region takes place during the winter anomaly (Garcia *et al.*, 1987); and a third one that relates the anomaly to a polar perturbation (Rapoport and Sinel'nikov, 1998).

Returning to our question set at the beginning of this introduction, we will investigate whether the inclination of the Earth's polar axis over the plane of the terrestrial orbit can have any connection with the winter anomalies. We know that such an axial tilt determines a different insolation over the two terrestrial hemispheres, hence producing a summer over the hemisphere which receives the larger insolation and a winter over the other one. Also, under the impact of the solar wind it generates an asymmetrical distortion of the geomagnetic field: its outskirts are more compressed in the summer hemisphere than in the winter one. The actual configuration of the geomagnetic field in the outer region at, say, the solstice times could be derived at the price of lengthy computations. For purpose of the present study it might be sufficient to adopt a simplified approach. We will hypothesize that the current sheet which determines the sunward boundary of the magnetosphere and which is produced by the impact of the solar wind with the field of the geomagnetic dipole be plane. Such a hypothesis is similar to that illustrated by Ratcliffe (1972, p. 69), but in the present case the direction of the geomagnetic dipole will not be orthogonal to the direction of arrival of the solar wind, rather it will be oriented to make with the direction of arrival of the solar wind an angle – at solstice – of $(90° + 23.5°)$. In this respect, the adopted approximation would be even more crude than that of Ratcliffe.

It should be understood that in our case as in the case studied by Ratcliffe, to speak of a definite angle, with respect to the axis of the geomagnetic dipole, of the direction of arrival of

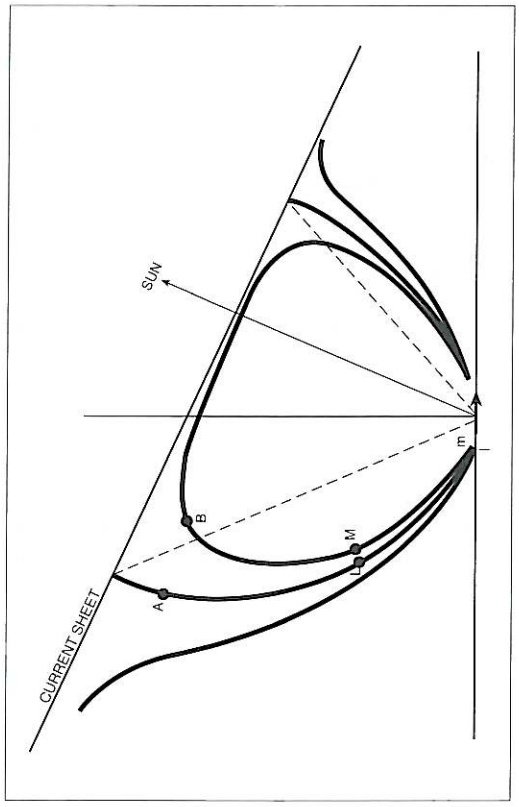

Fig. 1. Geomagnetic field lines of flux distorted by the action of the solar wind at solstice.

the solar wind is another simplification. The axis of the geomagnetic dipole does not coincide with the Earth's polar axis. Then, as the Earth rotates around its polar axis, the angle of arrival of the solar wind as seen from the geomagnetic dipole assumes a rather fuzzy connotation. Then the results of our analysis carried out with a solstitial angle exactly equal to $(90° + 23.5°)$ are affected by another approximation.

Computations carried out according to the hypothesis just described, led to the results depicted in fig. 1. The procedure was as follows. Reference is made to the sketch of fig. 2, where the arrow at the bottom represents the geomagnetic dipole and the arrow at the top represents its mirror image, produced by the current sheet: d is the distance between the two dipoles, χ is the angle between their directions. r and θ, r_1 and θ_1 are the polar co-ordinates of a generic point P, respectively referred to the geomagnetic dipole and to its mirror image. The present development is limited to the plane which contains the two dipoles. Then, if M is a quantity proportional to the dipole moment in question

$$\Phi(P) = M\cos\theta/r^2$$
$$\text{and} \quad \Phi_1(P) = M\cos\theta_1/r_1^2 \tag{1.1}$$

where Φ and Φ_1 are respectively the scalar po-

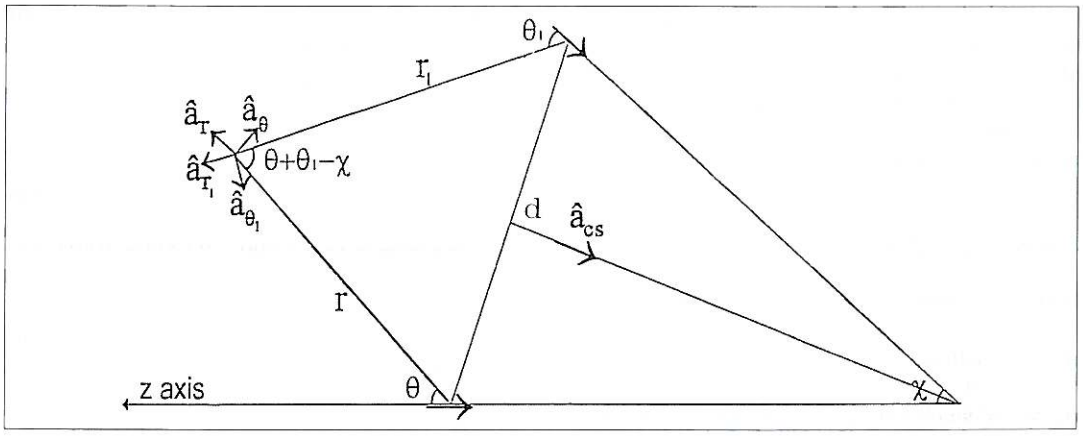

Fig. 2. Geomagnetic dipole and its mirror image.

tentials for the two magnetics fields. Hence, the resultant of the two is

$$\Phi_{TOT}(P) = M(\cos\theta/r^2 + \cos\theta_1/r_1^2). \quad (1.2)$$

Clearly, $r_1 = r_1\ (r,\theta)$ and $\theta_1 = \theta_1\ (r,\theta)$. Let's consider F the implicit function of r and θ given by the relation

$$F = M(\cos\theta/r^2 + \cos\theta_1/r_1^2) - \text{const} = 0 \quad (1.3)$$

which corresponds to an equipotential line. Its tangent is given by

$$-(\partial F/\partial\theta) : (r\partial F/\partial r) = +\,\partial r/r\partial\theta. \quad (1.4)$$

Hence, the tangent to the lines of flux will be:

$$(r\partial F/\partial r) : (\partial F/\partial\theta) = -\,r\partial\theta/\partial r. \quad (1.5)$$

If a succession of segments tangent to a line of flux is drawn on the basis of this last expression, an approximate representation of that line of flux can be obtained. Such was the procedure that was followed in order to obtain the plot of fig. 1. At this point a warning is in order. The field under examination is a tridimensional one, then the spacing between lines of flux is not in itself an indication of the field strength. In the present case one has to think in terms of tubes of flux, whose width is not constant. On the reflecting surface, *i.e.* at the current sheet, the field strength could be at most twice the strength of the field that would exist in the absence of the mirror. The validity of the plot of fig. 1 is that it allows a coup d'oeil of the direction of the composite magnetic field. Whenever the field intensity is needed, it will be necessary to proceed according to the following formulas:

$$r_1^2 = [r^2 + d^2 - 2rd\sin(\theta - \chi/2)] \quad (1.6)$$

$$\cos\theta_1 = [\cos(\theta - \chi) + (d/r)\sin(-\chi/2)]r/r_1 \quad (1.7)$$

$$\hat{a}_{r1} = \hat{a}_r\cos(\theta + \theta_1 - \chi) - \hat{a}_\theta\sin(\theta + \theta_1 - \chi) \quad (1.8)$$

$$\hat{a}_{\theta 1} = -\hat{a}_r\sin(\theta + \theta_1 - \chi) - \hat{a}_\theta\cos(\theta + \theta_1 - \chi) \quad (1.9)$$

$$\underline{B} = (M/r^3)(\hat{a}_r 2\cos\theta + \hat{a}_\theta\sin\theta) \quad (1.10)$$

$$\underline{B}_1 = (M/r_1^3)(\hat{a}_{r1}2\cos\theta_1 + \hat{a}_{\theta 1}\sin\theta_1) \quad (1.11)$$

$$\underline{B}_{TOT} = \underline{B} + \underline{B}_1 \quad (1.12)$$

where the symbols are those of fig. 2 and the B's indicate the magnetic fields.

If $\hat{a}_{cs}$ is the unit vector tangent to the current sheet, the following equation can be used for the determination of the two singular points in the plot of fig. 1, which are characterized by $B_{TOT} = 0$, because the intensity of the geomagnetic field and the intensity due to the mirror image dipole are equal and opposite. The solutions in term of θ of the equation

$$(\hat{a}_r 2\cos\theta + \hat{a}_\theta\sin\theta)\cdot\hat{a}_{cs} = 0 \quad (1.13)$$

are the co-ordinates of the those two points where the lines of flux land perpendicularly on the current sheet. Specifically, at solstices, the above equation becomes

$$(\hat{a}_r 2\cos\theta + \hat{a}_\theta\sin\theta)\cdot[-\hat{a}_r\cos(\theta - 23.5°) + \quad (1.14)$$

$$+\,\hat{a}_\theta\cos(90° - \theta + 23.5°)] = 0$$

which yields the two solutions

$$65° < \theta < 66° \quad \text{and} \quad 137° < \theta < 138°.$$

If the separation between the two dipoles is $2 \times 10 \times \cos(23.5°) = 2 \times 9.17$. the Earth radius being the unit of distance, then r for the first of the two values found is

$$9.17/\cos(90° - 65.5° + 23.5°) = 13.70$$
Earth's radii

and r for the second of the two values found is

$$9.17/\cos(137.5° - 90 + 23.5°) = 10.04$$
Earth's radii.

Then $B_{TOT} = 0$ at the two points whose co-ordinates are

$$r \approx 13.70, \quad 65° < \theta < 66°$$

and

$$r \approx 10.04, \quad 137° < \theta < 138°.$$

The plot of fig. 1 was obtained, as indicated above, by an iterative utilization of the following formulas:

$$\frac{-rd\theta}{dr} = \frac{\frac{r\partial F}{\partial r}}{\frac{\partial F}{\partial \theta}} = \frac{B_{\text{tot}}\big|_r}{B_{\text{tot}}\big|_\theta} = \tag{1.15}$$

$$= \frac{r\left\{\frac{-2\cos\theta}{r^3} + \frac{\cos(\theta-\chi)}{r_1^3} - \frac{3r^2\cos(\theta-\chi)}{r_1^5} - \frac{3rd\sin\left(-\frac{\chi}{2}\right)}{r_1^5} + \frac{3d^2\sin\left(-\frac{\chi}{2}\right)\sin\left(\theta-\frac{\chi}{2}\right)}{r_1^5} + \frac{3rd\cos(\theta-\chi)\sin\left(\theta-\frac{\chi}{2}\right)}{r_1^5}\right\}}{\left\{-\frac{\sin\theta}{r^2} - \frac{r\sin(\theta-\chi)}{r_1^3} + \frac{3r^2d\cos(\theta-\chi)\cos\left(\theta-\frac{\chi}{2}\right)}{r_1^5} + \frac{3r^2d\sin\left(-\frac{\chi}{2}\right)\cos\left(\theta-\frac{\chi}{2}\right)}{r_1^5}\right\}}.$$

This last result can be reached either starting from

$$F = M\left(\frac{\cos\theta}{r^2} + \frac{\cos\theta_1}{r_1^2}\right) - \text{const} = 0 \tag{1.16}$$

or starting from

$$\underline{B}_{\text{tot}} = \left(\frac{M}{r^3}\right)(\hat{a}_r 2\cos\theta + \hat{a}_\theta \sin\theta) + \tag{1.17}$$

$$+\left(\frac{M}{r_1^3}\right)(\hat{a}_{r1} 2\cos\theta_1 + \hat{a}_{\theta 1}\sin\theta_1).$$

If the two dipole's arrows taken into consideration were diverging rather then converging, the sign in front of χ should be + instead of –.

2. Interplay of geomagnetism, solar wind and galactic cosmic rays

Following the development of the preceding section, we may formulate a more specific question: can the magnetic field, outwardly distorted by the solar wind, as shown in fig. 1, be responsible for the existence of the winter anomalies? In the deformed dipole field of fig. 1 we distinguish three portions: a compressed portion near the equator and two depressed portions, not at the poles as in the case of an undisturbed dipole, but at about 75° of latitude north and south. The compressed portion will determine the small winter anomaly and this problem will be studied in Subsection 2.1. The depressed portion located in the winter hemisphere will determine the classic winter anomaly and this problem will be discussed and analyzed in Subsection 2.2. In the Appendix attached to the end of the paper the determination of Γ, the coefficient of collisional detachment of the electrons from the ions O_2^-, will be outlined, being a direct consequence of the data discussed in this Section 2 and yielding some information utilized in this Section 2.

The experimental support to our deductions was taken from the papers published in the issue of the *Journal of Atmospheric and Terrestrial Physics*, vol. 41, number 10/11 of October/November 1979, since they present the still more panoramic and rich collection of data on our specific subject. Such data are those obtained

during the Western European *D*-region Winter Anomaly Campaign 1975/1976 and can be compared with the simultaneous data relative to the solar wind, reported in the publication *Solar-Geophysical Data* published by the Center A for Solar-Terrestrial Physics in Boulder, Colorado.

2.1. *60-40 km heights*

We will study the formation of the lower part of the *D*-region even in presence of the winter anomaly. It is well known that the bottom of the *D*-region of the ionosphere is generated by the galactic cosmic rays which ionize the low atmosphere under the control of the geomagnetic field. Velinov (1968) carried out a detailed analysis of such a process. Starting from the Bethe-Block formula of the ionization by charged particles and utilizing the results of Störmer's theory on the propagation of energetic ions into the geomagnetic field (1955, Part II, Ch. I), he arrived at the following expression based on the *isotropic distribution of galactic cosmic rays*

$$q(h) = 1.8 \cdot 10^5 \rho(h) n_p(> R_c)(1nR_c + 4.15) \quad (2.1)$$

where: q = rate of ionization; h = altitude; ρ = atmospheric density, $n_p(> R_c)$ = integral spectrum of protons with a rigidity larger than R_c. In turn, R_c is the critical rigidity of protons given by Störmer as $R_c = 14.9 \cos^4 \lambda_m$ BeV, where λ_m is the geomagnetic latitude.

Expression (2.1) was derived for the case of an undisturbed geomagnetic field, represented as a dipole field. In our case we are dealing with the ensemble of two dipole fields: the undisturbed geomagnetic field and its mirror image that together bring about the field of fig.1.

The reconstruction of Störmer's theory on the basis of two dipoles rather than a single one would lead to very cumbersome equations. We suggest a simplified approach. In place of the application of Störmer's theory to the two dipoles operating simultaneously, we suggest the application of Störmer's theory to two dipoles that operate in succession, one after the other. We plan to examine situations at the solstice times. The operational scheme is that illustrated

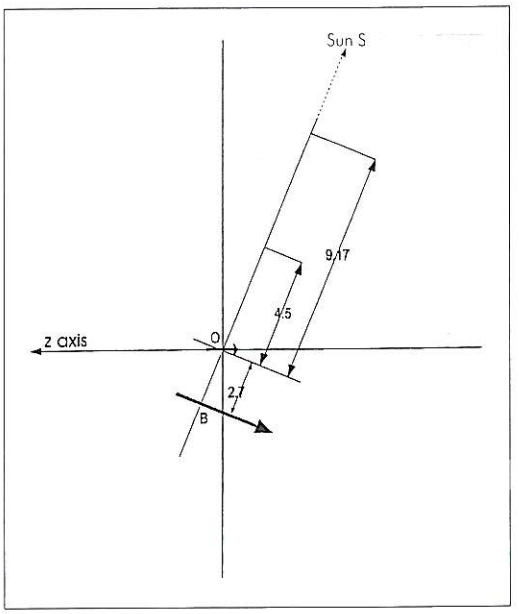

Fig. 3. Operational scheme with two dipoles. Dipole at B operates first; dipole at O operates afterwards.

in fig. 3. The geomagnetic dipole is located at O, near the center of the Earth; an associated imaginary dipole is located at B, it has a strength four times that of the geomagnetic dipole, it is at 2.7 Earth's radii from O along the straight line which makes, at the solstice time, an angle of 113.5° with the axis of geomagnetic dipole, in the antisolar direction, and is oriented normally to such a straight line OB. In moving along the direction SO (Sun-Earth), an energetic particle encounters at the point marked 9.17 (distance from O in terms of Earth's radii) a field due only to the dipole located at B, which is equal to the field produced by the geomagnetic dipole and by its image distant 2×9.17 Earth's radii. Proceeding from that point marked 9.17 to the point marked 4.5 (Earth's radii), the particle finds only the field of the dipole located at B, which is almost the same as the transversal component of the field due to the geomagnetic dipole at its image. From the point marked 4.5 (Earth's radii) to 1 (Earth's radius) the particle experiences only the field of the geomagnetic dipole, the contribution of the image dipole, at a first ap-

proximation, being negligible. Then – with respect to the galactic cosmic rays arriving along the direction (S-9.17-4.5-1) – we propose applying Störmer's formulas made valid for the dipole located at B, over the stretch (9.17-4.5) and the same Störmer's formulas made valid for the geomagnetic dipole located at O over the stretch (4.5-1) Earth's radii. Clearly, it is a crude approach, but it can yield some information on the influence of the field compression shown in fig. 1 over the trajectories of the incoming cosmic rays.

The plot in fig. 1 was obtained by putting the current sheet that bounds the magnetosphere at a distance of 9.17 Earth's radii from the Earth's center, where

$$\underline{B}|_{9.17} = \frac{-\mu_0 M_0}{4\pi r^3}(\hat{a}_r 2\cos 113.5° + \hat{a}_\theta \sin 113.5°) =$$

$$= \frac{-4\pi \cdot 10^{-7} \cdot 8.06 \cdot 10^{22}}{4\pi(9.17 \cdot 6.371)^3 \cdot 10^{18}}(-\hat{a}_r 0.797 + \hat{a}_\theta 0.917).$$

Hence, $\underline{B}_{tot}|_{9.17} = -7.413 \cdot 10^{-8}\,\hat{a}_\theta$. At the magnetopause, where the current sheet is located,

$$nmv^2 = \frac{B_{tot}^2}{2\mu_0} \qquad (2.2)$$

(Ratcliffe, 1972, p. 66) which says that the kinetic pressure of the solar wind (with mass of the particles m, velocity v and concentration n) is equal to the magnetic pressure. It emerges that, in our case, $nmv^2 = 2.186 \cdot 10^{-9}$, corresponds to an energy density of $1.093 \cdot 10^{-9}$ J/m^3. The energy density of solar wind is not a constant quantity, but changes significantly, especially at times of winter anomaly, as indicated by its measurements obtained by the spacecraft IMP 7 and IMP 8 and published monthly in the publication *Solar-Geophysical Data* of NOAA, being occasionally smaller and occasionally larger than $1.093 \cdot 10^{-9}$ J/m^3. Figure 4 supplies information on the characteristics of solar wind for January 1976. When the energy density is much smaller than $1.093 \cdot 10^{-9}$ J/m^3 the boundary between the domain of the dipole at B and the domain of the dipole at O in fig. 3 will have to be shifted to larger values than 4.5 Earth's radii. *Vice versa*, when the energy density is much larger than $1.093 \cdot 10^{-9}$ J/m^3 the boundary between the domain of the dipole at B and the domain of the dipole at O in fig. 3 will have to be shifted to smaller values than 4.5 Earth's radii.

In the present attempt to gain some understanding of the impact of the galactic cosmic rays on the lower atmosphere, the proposed duplexed use of Störmer's formulas will be extended to all directions included in a cone with a vertex in O, an axis making an angle of 113.5° (at solstice) with the axis of the geomagnetic dipole, and a cross section at about 9.17 Earth's radii from O which will cover the flattened portion of the magnetic field seen in fig. 1.

Equation (2.1) was based on the isotropic distribution of the galactic cosmic rays entering a dipole field. We will show evidence that – under specific conditions – the galactic cosmic rays that traverse the field of the dipole at B and are delivered to the field of the dipole at O, in fig. 3, are and remain concentrated in the summer hemisphere of the Earth. The starting point will be the following equation from Störmer (1955, p. 229)

$$\sin\theta = \left(\frac{2\gamma}{R} + \frac{R}{r^3}\right) \qquad (2.3)$$

where: θ = angle between the direction of motion of an energetic ionized particle and the meridian plane; γ = integration constant, which can assume the values from $-\infty$ to $+\infty$, but is limited to the range $-1 < \gamma \leq 0$ for particles which can move up to the position of geomagnetic dipole from infinity; R = cylindrical coordinate of position of the incoming particle in a system R, φ, z; where z is in the direction of the dipole located at the origin of the system with the South Pole pointing in the $+z$ direction; $r = (R^2 + z^2)^{1/2}$. In eq. (2.3) R and z are given in terms of the following unit of length:

$$C_{st} = \text{the Störmer's constant} = \left(\frac{\mu_0 e M_0}{4\pi m v}\right)^{1/2}$$

where: μ_0 = permittivity of the free space = $= 4\pi \cdot 10^{-7}$ henry per meter; e = particle's charge

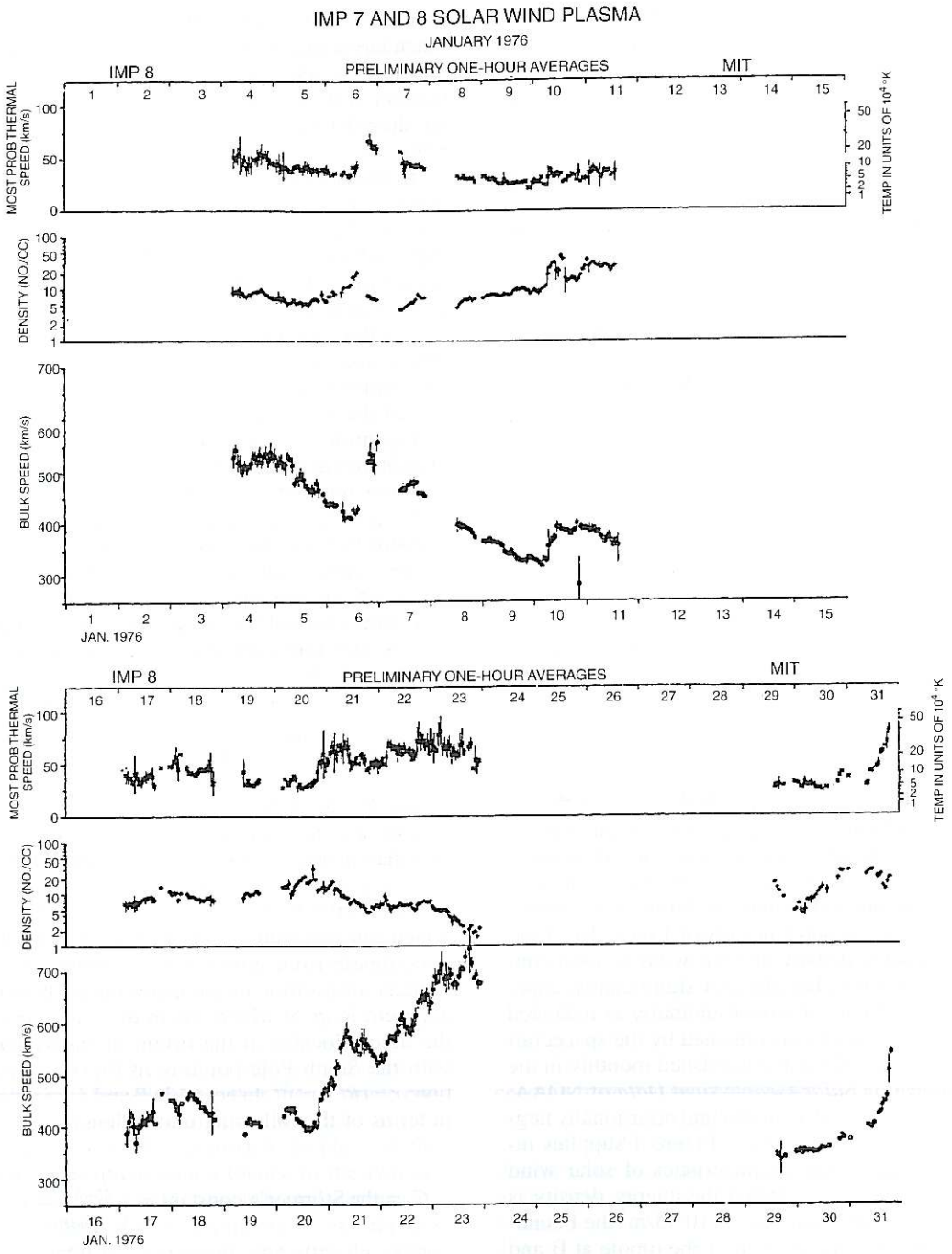

Fig. 4. Solar wind plasma recorded by IMP 7 and IMP 8 in January 1976. After *Solar-Geophysical Data*, 383 part II, July 1976, U.S. Department of Commerce (Boulder, Colorado, U.S.A. 80302).

in coulomb; M_0 = Earth's dipole moment = $= 8.06 \cdot 10^{22}$ Am^2; m = particle's mass in kg; v = particle's speed in m/s, and the SI system of units is used. C_{st} is seen to be a function of the rigidity of a particle, which is given as mvc when expressed in eV.

The meaning of the constant γ can be deduced if $\sin\theta$ is written as $\left(R\frac{d\varphi}{ds}\right)$, where $ds = vdt$, *i.e.* a quantity proportional to the differential time, since v is a constant. Then $\left(R\frac{d\varphi}{ds}\right)$ can be interpreted as the component of the velocity along the tangent to the circle drawn round the z-axis through the instantaneous position of the particle.

It follows that

$$R^2 \frac{d\varphi}{ds} = 2\gamma + \frac{R^2}{r^3}. \qquad (2.4)$$

At a great distance with respect to C_{st}, the ratio (R^2/r^3) is negligible and (2γ) can be interpreted as the moment of the momentum of the particle in the direction of the dipole axis, since (2.4) becomes

$$R^2 \frac{d\varphi}{ds} \approx 2\gamma. \qquad (2.5)$$

Equation (2.3) takes a more useful form when the geomagnetic latitude, λ_m, is evidenced, *i.e.*

$$\sin\theta = \frac{2\gamma}{r\cos\lambda_m} + \frac{\cos\lambda_m}{r^2}. \qquad (2.6)$$

Of course, λ_m assumes its true meaning when r equals the radius of the Earth. The relation $R_c = 14.9\cos^4\lambda_m$ BeV given by Störmer is obtained from eq. (2.6) when r is expressed as the ratio (radial distance from the Earth's center/C_{st}), the radial distance from the Earth's center is 6371 km, $\sin\theta = 0$, and $\gamma = -1$. In a more general case, it follows from eq. (2.6) that $R_c = (14.9/\gamma^2)\cos^4\lambda_m$ BeV, valid when the radial distance from the Earth's center is 6371 km, $\sin\theta = 0$ and $\gamma \neq -1$. At a first approximation, we take 6371 km as the distance of the lower D-region from the center of the Earth. It is clear that the particles of a given rigidity, being $-1 < \gamma \leq 0$ as reported above, will reach the lowest possible value of λ_m when $\gamma = -1$. To fix the ideas we will look for particles reaching $\lambda_m = 42°$, the geomagnetic latitude of some winter anomaly observations. In order to pick up a value of mvc, necessary to utilize the eq. (2.6) and to study the motion of the energetic ions, we should ask ourselves a preliminary question: can we expect to have particles of $\gamma = -1$ reaching the bottom of the D-region? In the case of a simple dipole the answer is «yes». But in the case of the two dipoles of fig. 3 operating in succession the answer is not always positive. One can be convinced of that by making a sequential utilization of eq. (2.6) as done in the following. Then, if $|\gamma| < 1$ at the bottom of the D-region one should chose a value of the rigidity larger than 14.9 $\cos^4$ (42°) BeV if the geomagnetic latitude of 42° is to be reached by the ionized particles. How much larger? The difficulty arises from the fact that the choice of the value of the rigidity of the particles, which is necessary at the beginning in order to start the computations, can be checked only at the end of the computations themselves. Only a cut and try approach leads to a satisfactory solution of the problem. This way was followed to study the motion of energetic protons that could reach a geomagnetic latitude of 42° at the bottom of the D-region when the scheme of fig. 3 is operative. Then $R_c = 5.3$ BeV.

Being $R_c = 5.3$ BeV, with the help of eq. (2.6) we can analyze the motion of energetic ionized particles in the scheme of fig. 3. We will have to deal not only with the quantities $\theta, \lambda_m, r, \gamma$ and C_{st} pertinent to the dipole located at O, but also with the corresponding quantities pertinent to the dipole located at B. A subscript t will be used for these latter. We shall deal with $\theta_t, \lambda_{mt}, r_t, \gamma_t$ and C_{stt}. The procedure to be adopted will be as follows: a point will be picked up arbitrarily, on account of the spatial isotropy of the galactic cosmic rays, at the boundary that separates the space where the dipole at B is considered to be operative from the space where the dipole at O is considered to be operant, *i.e.* the circumference with center at O and radius of 4.5 Earth's radii, which henceforth will be called «the boundary». First, eq. (2.6) will be utilized to compute θ_t as a function of the arbitrary value of λ_{mt} and of

$\gamma_t = -1$; r_t is determined once λ_{mt} on the boundary is chosen. Secondly, eq. (2.6) will be utilized to derive the value of γ, after having equated θ with θ_t; the radial distance r and the latitude λ_m are co-ordinates of the same point on the boundary, but now seen from the dipole at O rather than the dipole at B. Note, a discontinuity marks the transition from r_t to r and from λ_{mt} to λ_m. This unrealistic discontinuity is the toll that must be paid for the simplification introduced with the scheme of fig. 3. Ultimately, the λ_m cutoff in the lower D-region can be obtained by a third utilization of eq. (2.6), where r is the radial distance of the lower D-region from the Earth's center, γ assumes the value determined with the second utilization of eq. (2.6) and $\theta = 0$.

The outlined procedure has been followed for the protons of $R_c = 5.3$ BeV. It led to the conclusion that at winter solstice the ionization at the bottom of the D-region, in the neighborhood of $\lambda_m \approx 42°$, is significantly less than that predicted by eq. (2.1), when the energy density in the solar wind is almost equal to $1.093 \cdot 10^{-9}$ J/m^3. This conclusion was reached on the basis of the following considerations. It was stated above that the procedure for the analysis of the ionization of galactic cosmic rays had to start by picking up an arbitrary point on the boundary between the space dominated by the dipole at B and the space dominated by the dipole at O. But if $\gamma_t = -1$, $r_t \approx 1$ on that boundary (please keep in mind that the value of r_t depends on the rigidity of the particles) and eq. (2.6) is used, it will emerge that the arbitrary choice is reduced to pick up a point of $\lambda_{mt} \approx 0°$. Any other choice of λ_{mt} (being $\gamma_t = -1$, $r_t \approx 1$) will yield values of θ_t that are imaginary, according to eq. (2.6). What does this mean? Points for $\gamma_t = -1$, $r_t \approx 1$ and λ_{mt} significantly different from 0° are in the so called forbidden region envisaged by Störm-

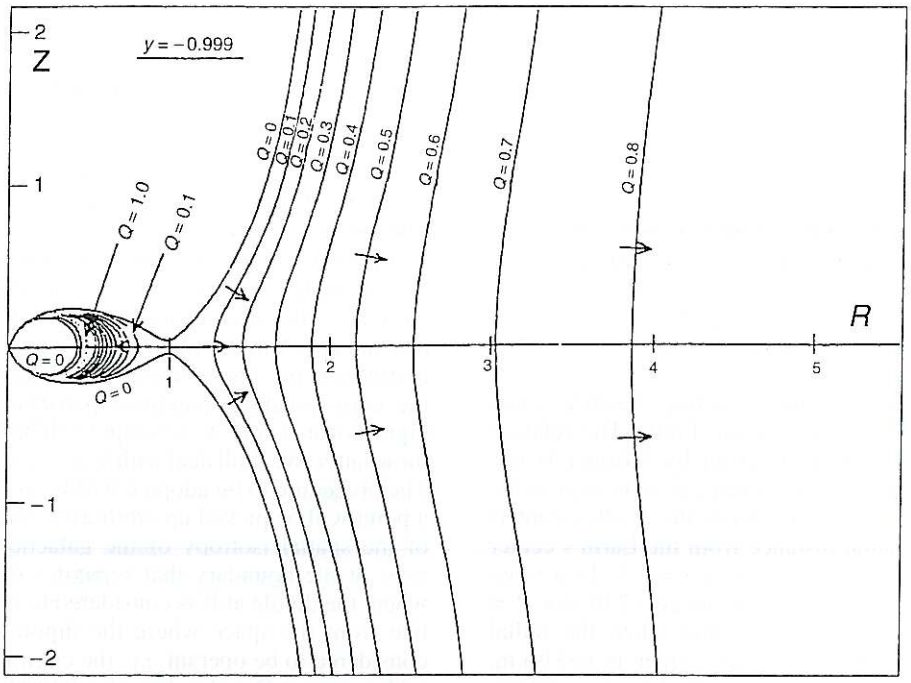

Fig. 5. Boundary between the allowed region and the forbidden region for the trajectories of ionized energetic particles moving in a dipole field when $\gamma = -0.999$. After Störmer (1955): *The Polar Aurora* (Clarendon Press), part II, p. 237.

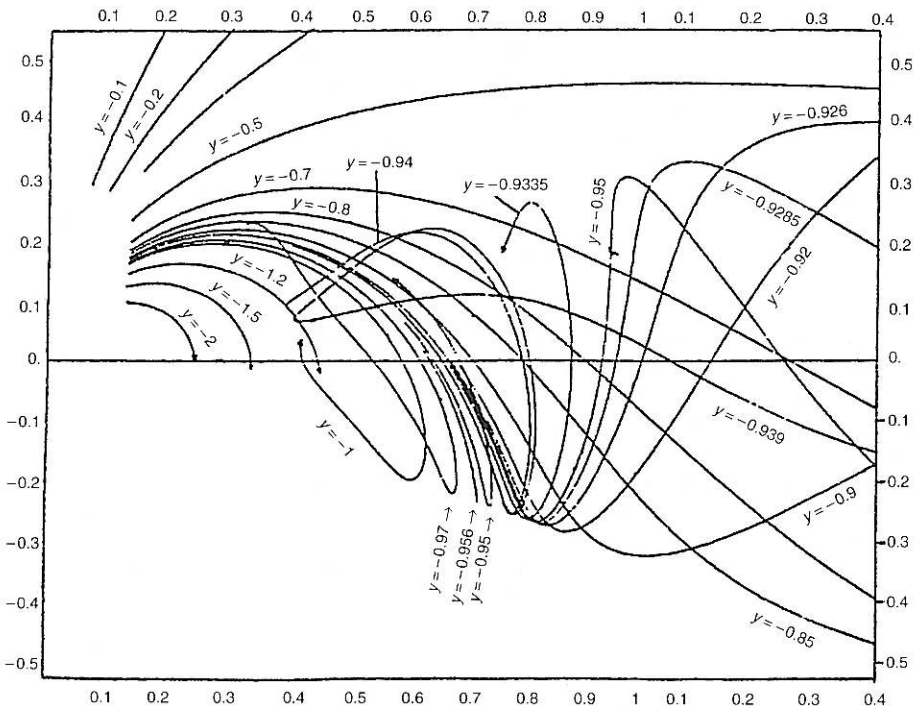

Fig. 6. Bundle of orbits through the origin in the *Rz*-plane. After Störmer (1955): *The Polar Aurora* (Clarendon Press), part II, p. 270.

er (1955, p. 231). He has shown that the ensemble of the trajectories of the incoming particles undergoes a kind of strangulation as they approach a point of $r_t = 1$, and that this strangling is more severe the closer γ_t is to its value – 1. As a matter of fact, at $\gamma_t = -1$ the width of the throttle is infinitesimal. Above and below $r_t = 1$ the ensemble of the trajectories is limited in a space which has the shape shown in fig. 5. Outside of this profile the trajectories cannot be found: it is the forbidden region.

Specifically, our computations carried out according to the procedure outlined above and based on the scheme of fig. 3 before the reduction imposed by the publication process, have yielded the following values: $C_{stt} = 2 \cdot C_{st} = 4.27 \cdot 10^7$ m; $r_{et} = 0.149$; r_t on the boundary equals $7.2 \cdot 0.149 = 1.07$; $\sin\theta_t = -1$ (for $\gamma_t = -1$, $r_t \approx 1$, and $\lambda_{mt} = 0°$); $\gamma = -0.928$ (for $\sin\theta = -1$, $r = 1.341$, and $\lambda_m = 23.5°$); $\lambda_{mo} = 42°$ at the bottom of the *D*-region.

These figures tell us that the field of the dipole located at B delivers to the field of the dipole located at O a flux of cosmic rays which is concentrated in the summer hemisphere of this last dipole. A question is in order. Will these cosmic rays be confined in the same summer hemisphere as they reach down the bottom of the *D*-region or will they spread over the two hemispheres? The answer can be deduced by looking at the fig. 6. Figure 6 plots the trajectories computed by numerical integrations of energetic particles having different γ's, which come from an infinite distance and reach the geomagnetic dipole located at the origin of the coordinates. Figure 6 shows that particles having values of γ between – 0.920 and – 0.9285 are to be found in the same hemisphere at *R* between 1.4 and 1, and at *R* between 0.5 and 0.2. Störmer (1955, p. 269) supports this result with a mechanical analogy and evidences that particles of γ between – 0.92 and – 0.93 have a similar be-

havior. In other words, our cosmic rays that were seen to arrive in the summer hemisphere at $r = 1.341$ will show up at the bottom of the *D*-region in the same summer hemisphere, hence producing a deficiency of ionization in the winter hemisphere, as pointed out above. This result is pertinent to a situation that can be schematized as in fig. 3, hence valid when the solar wind has an energy density almost equal to $1.093 \cdot 10^{-9}$ J/m^3.

The theoretical findings just illustrated receive experimental support from the data plotted in fig. 7. They were obtained during the Western Europe Winter Anomaly Campaign 1975/1976 by Widdel *et al.* (1979) and give the ambient ion density *versus* height in the range 60-40 km. The ion densities of January 4 and 6, 1976 are almost one order of magnitude less than the ion densities of January 21 and February 5, 1976. Such a difference cannot be explained as a consequence of a change in the influx of the galactic cosmic rays, which is known to be almost constant and subject only to a minor decrease in going from a minimum to a maximum of solar activity. Furthermore – very important – as shown in the Appendix the data of fig. 7 pertain to steady state conditions. The data of fig. 7 were not obtained at solstice time, but at dates a few weeks later. We think that a comparison between the findings of our theoretical analysis and these experimental results is still possible.

The data were obtained at a geomagnetic latitude quite close to 42°.

The information on the solar wind plasma of January 1976 reported in fig. 4 and the consecutive information for February 1976 (*Solar-Geophysical Data*, August 1976) indicate that the energy density was different from the value hypothesized in our theoretical analysis, namely $1.093 \cdot 10^{-9}$ J/m^3. Then the current sheet produced by the impact of the solar wind with the geomagnetic field has to be visualized at a distance from the Earth's center different from 9.17 Earth's radii. Let δ be such a distance of the current sheet. Straightforward computations, carried out with the procedure followed above, lead to the following values: $\delta = 8.699$ on January 4, 1976; $\delta = 8.842$ on January 6; $\delta = 7.87$ on January 21; and $\delta = 9.925$ on February 5. These values must be compared with the value of δ used for the construction of fig. 1, namely 9.17. Hence, the differences in percentages are: – 5% for January 4; – 3% for January 6; – 14% for January 21; and + 8% for February 5. The rela-

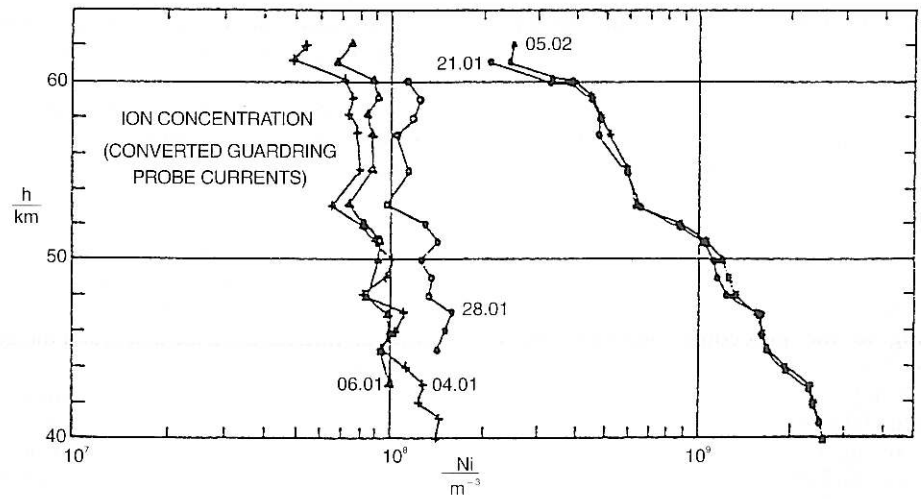

Fig. 7. Ion density *versus* height for January and February 1976. After Widdel *et al.* (1979): *J. Atmos. Terr. Phys.*, **41**, 1117.

tively small negative differences obtained for January 4 and 6 suggest that we can apply to the recordings on those dates the conclusion reached at the end of our theoretical analysis that was based on the situation depicted in fig. 1, precisely that the flux of galactic cosmic rays was preferentially shifted to the summer hemisphere, then producing a deficiency in the winter hemisphere. On the other hand, a different conclusion applies for the data of January 21 and February 5. Then the ionization almost predicted by eq. (2.1) was produced by the flux of the galactic cosmic rays, the conditions destructive of their original isotropic distribution being not verified.

This is what we see in fig. 7. Specifically, the rate of ionization at 60 km height, $\lambda_m = 42°$, according to eq. (2.1), with $n(42) = 7.8 \cdot 10^{-2}$ protons/cm^2 s ster (Velinov, 1968) and $\rho = 2.57 \cdot 10^{-7}$ g/cm^3 (from Houghton, 1979, p. 175), is $2.09 \cdot 10^4$ electrons/m^3 s. The Appendix reports that, at 60 km height, the negative-ion-to-electron ratio is found to be $\lambda = 5.63$ and the effective recombination coefficient is found to be $\alpha_e = 8 \cdot 10^{-12}$ m^3/s. Then, over there $N^- + N^+ = 6.25 \cdot 10^8$ ions/m^3. Similarly, at 40 km height, $\lambda_m = 42°$, according to eq. (2.1), with $n(42)$ as above and $\rho = 3.56 \cdot 10^{-6}$ g/cm^3 (from Houghton, 1979, p. 175), $q = 2.9 \cdot 10^5$ electrons/m^3 s. Being – see the Appendix – $\lambda = 230$ and $\alpha_e = 9.6 \cdot 10^{-9}$ m^3/s, then over there $N^- + N^+ = 2.53 \cdot 10^9$ ions/m^3. In fig. 7 $N^- + N^+ = 4 \cdot 10^8$ ions/m^3 at 60 km height and $N^- + N^+ = 2.5 \cdot 10^9$ ions/m^3 at 40 km height.

The limited, but definite discrepancy between the computed and the experimentally observed ion densities near 60 km height may be due to the fact that the steady state conditions valid for most of the interval 60-40 km heights, as indicated in the Appendix, were not verified near 60 km height. In any case, it seems that the experimental results give a solid support to our theoretical findings.

A brief comment is needed to explain how a difference in the δ's of only + 8% for the case of February 5 can be sufficient to bring the ionization process in line with eq. (2.1). For that date we should construct a scheme analogous to that of fig. 3 in order to carry out an examination similar to that carried out above. In such a case we must separate the domain of dipole at B from the domain of the dipole at O with the same criteria of approximation used to establish the scheme of fig. 3. Then, the boundary will not come out at a distance from O of 4.5 Earth's radii: it will be at a larger distance. The throttle that affects the propagation of cosmic rays in the domain of dipole at B will still be located at $r_t \approx 1$, again almost on the circumference of radius 4.5 Earth's radii. On the new boundary, r_t will be larger than 1. A glance at fig. 5 will tell us that then the cosmic rays will be delivered to the domain of the dipole at O being spread over a large stretch of latitudes. Furthermore, the new γ's will be outside the privileged range – 0.920 to – 0.930 stated above. Hence hemispheric anisotropy will not be present. A similar conclusion can be reached for the case of January 21. Then the boundary between the domain of the dipole at B and the domain of the dipole at O will be nearer to the Earth's center than in fig. 3. Again the hemisphere anisotropy will be absent.

It remains to be said that Widdel *et al.* (1979) stated that no change in the intensity of cosmic ray radiation was measured at the ground during the Winter Anomaly Campaign. In our theoretical analysis, it was shown that the hemispheric anisotropy in the ionization of the lower *D*-region was related to the condition of having $r_t \approx 1$ on the boundary at 4.5 Earth's radii from the Earth's center. Particles that reach the ground level at $\lambda_m \neq 42°$ would have to be either more or less energetic that those of $R_c = 5.3$ BeV. Then r_{et} will be different from 0.149 and hence r_t different from 1 at 4.5 radii from Earth's center. Hence, no anisotropy should be expected and no changes in the intensity of the cosmic radiation should be detected.

2.2. *90-70 km heights*

We will try to show how the distorted geomagnetic field, as sketched in fig. 1, gives way to a series of events that lead to an enhancement of the electron density in the upper *D*-region of the ionosphere at low latitudes, hence to an enhancement of the absorption of the radio waves which primarily goes under the name of winter anomaly. Our attention will be focussed not on the flat, compressed portion of the distorted

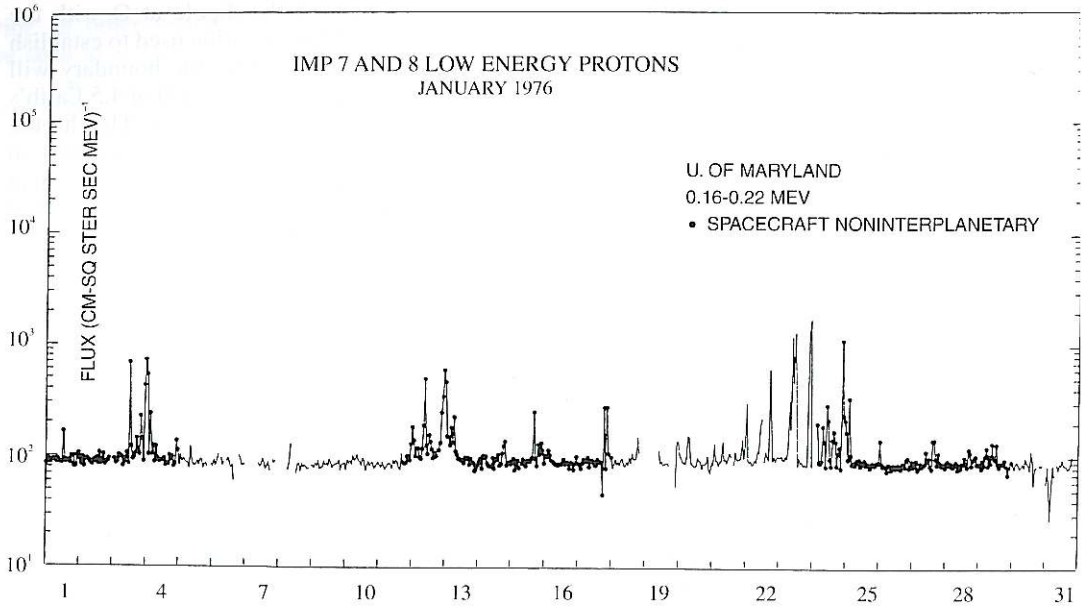

Fig. 8. Flux of low energy protons, between 0.16 and 0.22 MeV observed by IMP 7 and IMP 8 in January 1976. After *Solar-Geophysical Data*, 383 part II, July 1976, U.S. Department of Commerce (Boulder, Colorado, U.S.A. 80302).

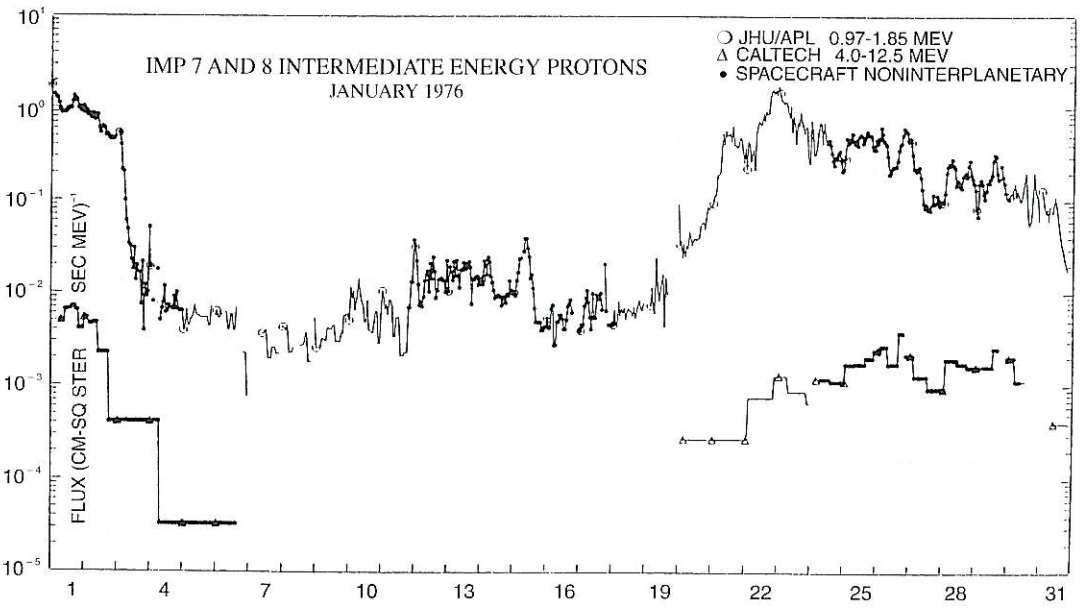

Fig. 9. Flux of low energy protons, between 0.97 and 1.85 MeV observed by IMP 7 and IMP 8 in January 1976. After *Solar-Geophysical Data*, 383 part II, July 1976, U.S. Department of Commerce (Boulder, Colorado, U.S.A. 80302).

geomagnetic field, as in Section 2.1, but rather on the high latitude portion of that field, in proximity of the singular points where $B_{TOT} = 0$. There we envisage the formation of what we may call magnetic funnels, through which particle fluxes of solar origin can go through and can be conveyed. Indeed, near the points where $B_{TOT} = 0$ the lines of the distorted geomagnetic flux are almost parallel to the direction of arrival of particles from the sun.

The series of events that will be studied is: 1) influx of «super» solar wind; 2) transit of this «super» solar wind though the quoted geomagnetic funnels and its intensification; 3) perturbation produced by this «super» solar wind on the circulation of the atmospheric polar vortex at $\approx$ 100 km height; 4) consequent equatorward outflow of arctic (alternatively antarctic) air with its content of auroral N0; 5) enhancement of electron density in the low latitude of the upper *D*-region due to the low ionization potential of N0.

2.2.1. Figures 8 and 9 present sets of data that are simultaneous with a winter anomaly event listed in table I. Figures 8 and 9, taken from the publication *Solar-Geophysical Data*, display recordings of energetic particle flux for the month of January 1976, obtained by the NASA spacecrafts IMP 7 and IMP 8. This flux is a kind of a «super» solar wind superimposed on the bulk of a basic solar wind, primarily constituted by protons of average energy of 500 eV (fig. 4). Unfortunately, only two stretches of the data collected during that month can be used for our analysis since the satellites were operating outside the magnetotail of the Earth's magnetosphere, hence in the interplanetary space, only for a limited number of days. Fortunately, usable records for the days from January 17 to January 24 are available. From table I we can gather that on those days a strong enhancement of radio waves absorption was detected, denouncing the presence of a winter anomaly event. It seems rather significant that, in coincidence with the inception of a strong winter anomaly event on January 21, the records show a definite upsurge of energetic particle flux on the same date. For an understanding of the data of figs. 8 and 9 the following explanatory note is reported (*Solar-Geophysical Data*, February 1976): «Fluxes in units of $(cm^2 \text{ ster } s)^{-1}$ have been obtained by folding together count rates, geometric factors, and, when appropriate, pulse height analysis data. These fluxes are then divided by the width of the energy window to yield the differential fluxes plotted».

Table I. Winter anomaly absorption. After Widdel *et al.* (1979). Electron densities during winter anomalous absorption of different intensity observed at 37.1°N, 6.73°W, during winter 1975/1976 - I. *J. Atmos. Terr. Phys.*, **41**, p. 1111.

Date	Zenith angle (degrees)	Absorption during launch (dB)
17.12.75	64.2	18.6
21.01.76	64.4	54.5
04.01.76	67.7	48.5
08.02.76	65.1	28.5
05.02.76	71.3	17.9
02.01.76	71.4	39.5
21.01.76	73.3	34.4
04.01.76	75.0	37.7
28.01.76	76.1	53.8
06.01.76	76.9	52.7
23.01.76	77.3	31.9
04.01.76	77.4	37.0
20.01.76	77.9	26.9
26.01.76	78.0	24.0
14.01.76	78.3	35.9
22.01.76	78.4	52.1
09.01.76	80.1	19.3
12.01.76	81.0	10.3

The geographic latitude of El Arenosillo (37.1°N) corresponds to the geomagnetic latitude, λ_m, of about 42°N.

It is important to notice that the fluxes of figs. 8 and 9, as they begin to show up, present a very chopped trend, which proves that they are highly anisotropic. The loss and recovery of the collimation by the recording instruments aboard the satellites are responsible for this effect.

2.2.2. The flux of the particles reported in figs. 8 and 9 can penetrate into the Earth's magnetosphere and ionosphere because it is almost parallel to the lines of flux of the distorted geo-